

Application of Polynomial Models in Bayesian Fusion of Humidity Sensors

Plamen Nikovski¹, Nikolay Doychinov¹

¹ *University of Food Technologies, 26 Maritza Blvd., 4002, Plovdiv, Bulgaria*

Abstract – Local polynomial trend models are a special class of state-space models that can be used without having the full information about the process under study, since most of their parameters are embodied in the state vector and estimated immediately. This makes them attractive for use in signal processing. The present work considers problems that arise when using a polynomial model with a local quadratic trend for Bayesian fusion of two humidity sensors. The unknown sensor biases make it impossible for the model to satisfy the observability conditions. There is currently no general solution to this problem. To overcome this difficulty, an approach is presented where the humidity measurement result implicitly includes the bias of one of the sensors.

The results of the study can be used to fuse quantities other than humidity when two or more sensors are available.

Keywords – humidity, sensor fusion, bias, Kalman, polynomial, model.

1. Introduction

Nowadays, autoregressive integrated moving-average (ARIMA) models [1] are one of the most commonly used to describe changes in environmental factors.

ARIMAs effectively capture the temperature and humidity course and provide a forecast with a small mean square error [2], [3]. Air quality [4], [5] and the levels of air pollutants such as carbon monoxide (CO), nitric oxide (NO), nitrogen dioxide (NO₂), sulphur dioxide (SO₂), ozone (O₃) and particulate matter [6],[7],[8], as well as the concentrations of pollen responsible for seasonal allergies [9], [10] have been successfully monitored by means of these models.

Typically, any stochastic process, and hence the one described by an ARIMA model, can be represented as the sum of two principal components [11]: a signal (trend) that describes a smooth underlying mean and a residual component, often considered as noise. Local Polynomial trend Models (PM) [12], [13] belong to this group. They have a number of unique properties that make them particularly suitable for representing different types of temporal data:

-PM describe a stochastic process with a polynomial trend. According to the Weierstrass theorem, any smooth curve (signal) defined on a finite interval can be arbitrarily well approximated by a polynomial [12]. In other words, in a short period of time for any ARIMA process, a PM with a similar trend can be found.

-PM is a linear model, but it can be used to approximate nonlinear stochastic processes.

-PM models have a unique state space representation where most of the model parameters are embodied in the state vector. The description of the classical ARIMA model includes three order parameters, n_p , n_d and n_q , which respectively define the number of autoregressive terms (AR), the number of differentiations applied and the number of moving average (MA) terms in the model, the $n_p + n_q$ coefficients associated with the AR and MA terms of the model and the variance of the innovation white noise [1]. In PM there is a parameter $(n - 1)$ defining the order of the polynomial model where n is the size of PM state vector and two other parameters known as the measurement noise intensity r and the process noise intensity q [12]. This greatly simplifies and even eliminates the need for PM identification.

DOI: 10.18421/TEM123-30

<https://doi.org/10.18421/TEM123-30>


Corresponding author: Plamen Nikovski,
*University of Food Technologies, 26 Maritza Blvd.,
4002, Plovdiv, Bulgaria*
Email: plmnn@abv.bg

Received: 01 June 2023.

Revised: 11 August 2023.

Accepted: 18 August 2023.

Published: 28 August 2023.

 © 2023 Plamen Nikovski & Nikolay Doychinov; published by UIKTEN. This work is licensed under the Creative Commons Attribution-NonCommercial-NoDerivs 4.0 License.

The article is published with Open Access at <https://www.temjournal.com/>

In this paper, a discrete model with a local quadratic trend, also known as a second-order polynomial model ($(n - 1) = 2$), is used to model stochastic processes [12]:

$$\mathbf{z}_k = \underbrace{\begin{pmatrix} 1 & \tau & 0,5\tau^2 \\ 0 & 1 & \tau \\ 0 & 0 & 1 \end{pmatrix}}_F \mathbf{z}_{k-1} + \boldsymbol{\zeta}_{k-1} \quad (1)$$

$$y_k = \underbrace{\begin{pmatrix} 1 & 0 & 0 \end{pmatrix}}_C \mathbf{z}_k + \eta_k$$

where $k = 1, 2, \dots$ is the discrete time, τ is the sampling period, \mathbf{z}_k is the process state vector, $C\mathbf{z}_k$ and y_k are the process-induced signal and its observation, $\boldsymbol{\zeta}_k$ and η_k are white noises with zero mean and covariance matrices

$$\mathbf{Q}_z = \begin{bmatrix} \frac{\tau^5}{20} & \frac{\tau^4}{8} & \frac{\tau^3}{6} \\ \frac{\tau^4}{8} & \frac{\tau^3}{3} & \frac{\tau^2}{2} \\ \frac{\tau^3}{6} & \frac{\tau^2}{2} & \tau \end{bmatrix} q, \quad q > 0 \quad (2)$$

and

$$\mathbf{R}_z = \frac{r}{\tau}, \quad r > 0 \quad (3)$$

The above mentioned features have increased the interest in PM models and their use in signal processing. This work considers the possibilities and proposes solutions to problems that arise when using a polynomial model with a local quadratic trend as an element of a Bayesian approach to humidity sensor fusion.

2. A Bayesian Approach to Sensor Fusion

The main challenge in designing a multi-sensor system is to choose an appropriate way to combine (fuse) the information from the sensors so that the final result is better than that obtained by using the same sensors individually [14], [15]. When it comes to extracting information from raw sensor data, which is generally imprecise, incomplete and uncertain probabilistic approaches and in particular Bayesian inference [16], [17] can be quite useful.

Assume that the measurement system (shown in Figure 1) is composed of two sensors S^1 and S^2 (the superscript denotes the sensor number) that monitor the same process MP:

$$\begin{aligned} y_k^1 &= f^1(u_k, v_k^1) \\ y_k^2 &= f^2(u_k, v_k^2) \\ u_k &= u(\mathbf{x}_k) \end{aligned} \quad (4)$$

where y_k^1, y_k^2 are available scalar sensor readings obtained from the first and second sensors respectively, f^1 and f^2 are functions representing

the measurement process models, \mathbf{x}_k is a real-valued n -dimensional vector that describes some useful information about the process MP (In general, \mathbf{x}_k can be augmented with variables, that are not related to MP but affect sensor readings, e.g. sensor biases), u_k is the input signal to the sensors, and v_k^1, v_k^2 are scalar zero-mean white noises (measurement noises).

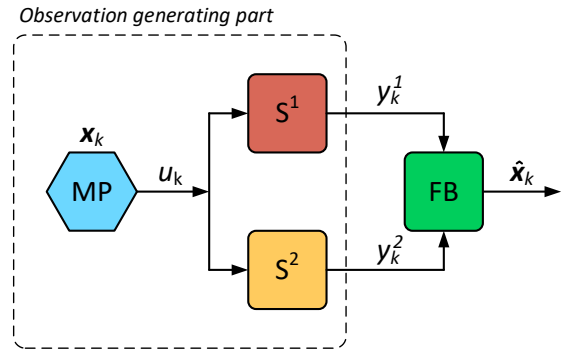


Figure 1. Block diagram of a measurement system with two sensors. The sensors S^1 and S^2 receive the signal u_k produced by the state \mathbf{x}_k of the monitored process MP. The fusion block FB executes an algorithm to compute an estimate $\hat{\mathbf{x}}$ of this state from the sensor measurements y_k^1 and y_k^2 .

The state \mathbf{x}_{k-1} evaluates to \mathbf{x}_k according to the equation:

$$\mathbf{x}_k = g(\mathbf{x}_{k-1}, \mathbf{w}_{k-1}) \quad (5)$$

where g is a function representing the state transition model, and \mathbf{w}_{k-1} is an n -dimensional zero-mean white noise vector (process noise). Let us denote the measurement sequences obtained from the sensors as follows:

$$\begin{aligned} y_{1:k}^1 &= \{y_1^1, y_2^1, \dots, y_k^1\} \\ y_{1:k}^2 &= \{y_1^2, y_2^2, \dots, y_k^2\} \end{aligned} \quad (6)$$

If \mathbf{x}_k is assumed to be a random variable, the data fusion problem can be viewed as a problem of estimating $p(\mathbf{x}_k | y_{1:k}^1, y_{1:k}^2)$, a conditional probability that represents all knowledge about the state \mathbf{x}_k in probabilistic terms considering all observations up to time k . Usually, the solution of this problem is sought under the following two well-known assumptions in probability theory [18], [19]:

-The sequence $\dots, \mathbf{x}_{k-2}, \mathbf{x}_{k-1}, \mathbf{x}_k, \dots$ is a Markov process. This means that for each time step k , \mathbf{x}_k depends only on \mathbf{x}_{k-1} :

$$p(\mathbf{x}_k | \mathbf{x}_{k-1}, y_{1:k-1}^1, y_{1:k-1}^2) = p(\mathbf{x}_k | \mathbf{x}_{k-1}) \quad (7)$$

but not on the previous state history.

-The measurements y_k^1, y_k^2 given the state \mathbf{x}_k are conditionally independent:

$$p(y_k^1, y_k^2 | \mathbf{x}_k, y_{1:k-1}^1, y_{1:k-1}^2) = p(y_k^1 | \mathbf{x}_k) p(y_k^2 | \mathbf{x}_k) \quad (8)$$

This means that the current sensor readings do not depend on each other, nor on past states or past measurements.

First, the current value of the state is estimated if only the measurements obtained at previous times are given. Considering (7), the law of total probability [20]

$$p(\mathbf{x}_k | y_{1:k-1}^1, y_{1:k-1}^2) = \int p(\mathbf{x}_k | \mathbf{x}_{k-1}, y_{1:k-1}^1, y_{1:k-1}^2) p(\mathbf{x}_{k-1} | y_{1:k-1}^1, y_{1:k-1}^2) d\mathbf{x}_{k-1} \quad (9)$$

can be rewritten as

$$p(\mathbf{x}_k | y_{1:k-1}^1, y_{1:k-1}^2) = \int p(\mathbf{x}_k | \mathbf{x}_{k-1}) p(\mathbf{x}_{k-1} | y_{1:k-1}^1, y_{1:k-1}^2) d\mathbf{x}_{k-1} \quad (10)$$

The Probability Density Function (PDF) $p(\mathbf{x}_k | \mathbf{x}_{k-1})$ is given by the equation of state (5) and the noise statistic \mathbf{w}_{k-1} . Now the current measurements y_k^1 and y_k^2 are used to update the a priori probability (10). Using Bayes' theorem under condition (8) we get the following result [18], [19]:

$$p(\mathbf{x}_k | y_{1:k}^1, y_{1:k}^2) = \frac{p(y_k^1 | \mathbf{x}_k) p(y_k^2 | \mathbf{x}_k) p(\mathbf{x}_k | y_{1:k-1}^1, y_{1:k-1}^2)}{p(y_k^1, y_k^2 | y_{1:k-1}^1, y_{1:k-1}^2)} \quad (11)$$

where $p(y_k^1, y_k^2 | y_{1:k-1}^1, y_{1:k-1}^2)$ is a normalization constant calculated by

$$p(y_k^1, y_k^2 | y_{1:k-1}^1, y_{1:k-1}^2) = \int p(y_k^1 | \mathbf{x}_k) p(y_k^2 | \mathbf{x}_k) p(\mathbf{x}_k | y_{1:k-1}^1, y_{1:k-1}^2) d\mathbf{x}_k \quad (12)$$

Here the likelihood functions of the two sensors $p(y_k^1 | \mathbf{x}_k)$ and $p(y_k^2 | \mathbf{x}_k)$ are defined by equations (4) and the known noise statistics v_k^1, v_k^2 . Equation (10) together with equation (11) allows the new estimate $p(\mathbf{x}_k | y_{1:k}^1, y_{1:k}^2)$ to be calculated recursively from the old estimate $p(\mathbf{x}_{k-1} | y_{1:k-1}^1, y_{1:k-1}^2)$ and the new measurements y_k^1, y_k^2 .

In most cases, no closed form solution exists for the integrals (10) and (12), making the Bayesian estimation procedure difficult to apply in practice. One way to overcome this problem is to approximate $p(\mathbf{x}_k | \mathbf{x}_{k-1})$, $p(y_k^1 | \mathbf{x}_k)$ and $p(y_k^2 | \mathbf{x}_k)$ with distributions obtained from linear Gaussian state and measurement models [19,21]:

$$\begin{aligned} \mathbf{x}_k &= \mathbf{F} \mathbf{x}_{k-1} + \mathbf{w}_{k-1} \\ y_k^1 &= \mathbf{H}^1 \mathbf{x}_k + v_k^1 \\ y_k^2 &= \mathbf{H}^2 \mathbf{x}_k + v_k^2 \end{aligned} \quad (13)$$

where \mathbf{F} is the transition matrix of size $(n \times n)$, $\mathbf{H}^1, \mathbf{H}^2$ are the measurement matrices of size $(1 \times n)$, $\mathbf{w}_{k-1} \sim N(0, \mathbf{Q})$, $v_k^1 \sim N(0, R^1)$ and $v_k^2 \sim N(0, R^2)$ are Gaussian noises, the initial state \mathbf{x}_0 is Gaussian $\mathbf{x}_0 \sim N(\hat{\mathbf{x}}_{0|0}, \mathbf{P}_{0|0})$, the variables $v_1^1, v_2^1, \dots, v_k^1, v_1^2, v_2^2, \dots, v_k^2$, the components of the vectors

$\mathbf{w}_0, \mathbf{w}_1, \dots, \mathbf{w}_{k-1}$ and the components of the state \mathbf{x}_0 are mutually uncorrelated. In this case, the predicted and posterior PDFs of the state are equal to [21]:

$$\begin{aligned} p(\mathbf{x}_k | y_{1:k-1}^1, y_{1:k-1}^2) &\sim N(\hat{\mathbf{x}}_{k|k-1}, \mathbf{P}_{k|k-1}) \\ p(\mathbf{x}_k | y_{1:k}^1, y_{1:k}^2) &\sim N(\hat{\mathbf{x}}_{k|k}, \mathbf{P}_{k|k}) \end{aligned} \quad (14)$$

where

$$\begin{aligned} \hat{\mathbf{x}}_{k|k-1} &= \mathbf{F} \hat{\mathbf{x}}_{k-1|k-1} \\ \mathbf{P}_{k|k-1} &= \mathbf{Q}_{k-1} + \mathbf{F} \mathbf{P}_{k-1|k-1} \mathbf{F}^T \\ \hat{\mathbf{x}}_{k|k} &= \hat{\mathbf{x}}_{k-1|k-1} + \mathbf{K}_k (\mathbf{y}_k - \mathbf{H} \hat{\mathbf{x}}_{k|k-1}) \\ \mathbf{P}_{k|k} &= \mathbf{P}_{k|k-1} - \mathbf{K}_k \mathbf{H} \mathbf{P}_{k|k-1} \\ \mathbf{K}_k &= \mathbf{P}_{k|k-1} \mathbf{H}^T (\mathbf{H} \mathbf{P}_{k|k-1} \mathbf{H}^T + \mathbf{R})^{-1} \\ \mathbf{y}_k &= (y_k^1 \quad y_k^2)^T \\ \mathbf{H} &= \begin{pmatrix} \mathbf{H}^1 & 0 \\ 0 & \mathbf{H}^2 \end{pmatrix}, \mathbf{R} = \begin{pmatrix} R^1 & 0 \\ 0 & R^2 \end{pmatrix} \end{aligned} \quad (15)$$

Algorithm (15), known as the Kalman Filter (KF), computes $\hat{\mathbf{x}}_{k|k}$ by minimizing the mean of squared Euclidean distance between the estimate value and the true value of the state vector given observations $y_{1:k}^1$ and $y_{1:k}^2$:

$$E \left[(\hat{\mathbf{x}}_{k|k} - \mathbf{x}_k)^T (\hat{\mathbf{x}}_{k|k} - \mathbf{x}_k) \middle| y_{1:k}^1, y_{1:k}^2 \right] \quad (16)$$

Thus, $\hat{\mathbf{x}}_{k|k}$ be considered as the result of sensor data fusion based on the concept that the best value of the state vector is its estimate in the Minimum Mean Squared Error sense (MMSE) [22], [23]. Intuitively simple and easy to implement, this approach is widely used in practice.

In the following we will assume that the pair of matrices (\mathbf{F}, \mathbf{H}) is observable [24]:

$$\text{rank} \begin{pmatrix} \mathbf{H} \\ \mathbf{H}\mathbf{F} \\ \vdots \\ \mathbf{H}\mathbf{F}^{n-1} \end{pmatrix} = n \quad (17)$$

Satisfying this condition allows to obtain a unique estimate $\hat{\mathbf{x}}_{k|k}$ of the state based on the observations obtained by the sensors.

3. Fusion of Humidity Sensors

Advances in Micro-ElectroMechanical Systems (MEMS) technology have made it possible to create compact, accurate and robust humidity sensors that allow a measurement system to be built quickly and easily. In most cases, the MEMS humidity sensor is a single chip combining a capacitive sensing element and electronics. The electrodes of the sensing element are sealed with a polymer (e.g. polyimide) which can absorb or release water molecules from or into the environment. Any change in relative humidity affects the dielectric permittivity of the polymer and hence the capacitance of the sensing element. An electronic circuit detects these changes and converts them into a digital output signal.

Due to their good results, capacitive MEMS sensors are not only preferred, but have been adopted as one of the industry standards for humidity measurement.

Capacitive MEMS humidity sensors are a special class of sensors, but like the others, their behaviour can be described reasonably well by the following equation [25], [26]:

$$y_k = u_k + e_k + v_k \quad (18)$$

In the following considerations, the sensor bias e_k is assumed to be a random process close to a Random Walk (RW):

$$e_k = e_{k-1} + \lambda_{k-1} \quad (19)$$

where λ_{k-1} is Gaussian white noise with zero mean, and humidity u_k is a signal generated by a polynomial process with a local quadratic trend. The latter means that the humidity can be represented as a linear combination of the components of the state vector \mathbf{z}_k :

$$u_k = \mathbf{C}\mathbf{z}_k \quad (20)$$

If we have two independent observations y_k^1, y_k^2 obtained according to equation (18) taking into account (1) it can be written:

$$\begin{aligned} \mathbf{z}_k &= \mathbf{A}\mathbf{z}_{k-1} + \boldsymbol{\zeta}_{k-1} \\ y_k^1 &= \mathbf{C}\mathbf{x}_k + e_k^1 + \eta_k^1 \\ y_k^2 &= \mathbf{C}\mathbf{x}_k + e_k^2 + \eta_k^2 \\ e_k^1 &= e_{k-1}^1 + \lambda_{k-1}^1 \\ e_k^2 &= e_{k-1}^2 + \lambda_{k-1}^2 \end{aligned} \quad (21)$$

This system of equations can be reduced to the form (13), where:

$$\mathbf{x}_k = \begin{pmatrix} \mathbf{z}_k \\ e_k^1 \\ e_k^2 \end{pmatrix}, \quad \mathbf{F} = \begin{pmatrix} \mathbf{A} & \mathbf{0} \\ \mathbf{0} & \mathbf{I} \end{pmatrix}, \quad \mathbf{w}_k = \begin{pmatrix} \boldsymbol{\zeta}_k \\ \lambda_k^1 \\ \lambda_k^2 \end{pmatrix}, \quad (22)$$

$$\mathbf{H}^1 = (\mathbf{C} \quad 1 \quad 0), \quad \mathbf{H}^2 = (\mathbf{C} \quad 0 \quad 1), \\ v_k^1 = \eta_k^1, \quad v_k^2 = \eta_k^2$$

Here the vector \mathbf{x}_k contains the unknown sensor biases in addition to the state variables representing the humidity. Unfortunately, the determination of \mathbf{x}_k by sensor fusion is impossible since the matrix pair (\mathbf{F}, \mathbf{H}) is unobservable [27], [28]. Let us try to find a solution to this problem by treating the sum of the actual humidity and the bias of one of the sensors, e.g. the first one, as some new humidity process u'_k :

$$\begin{aligned} u'_k &= u_k + e_k^1 \\ u'_k &= \mathbf{C}\mathbf{x}_k \end{aligned} \quad (23)$$

With two observations available, the equations (18), (1) and (23) lead to

$$\begin{aligned} \mathbf{z}_k &= \mathbf{A}\mathbf{z}_{k-1} + \boldsymbol{\zeta}_{k-1} \\ y_k^1 &= \mathbf{C}\mathbf{z}_k + \eta_k^1 \\ y_k^2 &= \mathbf{C}\mathbf{z}_k + d_k + \eta_k^2 \\ d_k &= d_{k-1} + \lambda_{k-1} \end{aligned} \quad (24)$$

where $d_k = e_k^2 - e_k^1$ and $\lambda_k = \lambda_k^2 - \lambda_k^1$. The system (24) can be written in the form (13) where

$$\begin{aligned} \mathbf{x}_k &= \begin{pmatrix} \mathbf{z}_k \\ d_k \end{pmatrix}, \quad \mathbf{F} = \begin{pmatrix} \mathbf{A} & \mathbf{0} \\ \mathbf{0} & 1 \end{pmatrix}, \quad \mathbf{w}_k = \begin{pmatrix} \boldsymbol{\zeta}_k \\ \lambda_k \end{pmatrix}, \\ \mathbf{H}^1 &= (\mathbf{C} \quad 0), \quad \mathbf{H}^2 = (\mathbf{C} \quad 1), \quad v_k^1 = \eta_k^1, \\ v_k^2 &= \eta_k^2 \end{aligned} \quad (25)$$

The model (13) with the matrices (25) is now observable. This means that \mathbf{x}_k (respectively \mathbf{z}_k and u'_k) can be estimated by fusing the information from the two observations with the algorithm (13). Unfortunately, the humidity u'_k obtained in this way is different from the true humidity u_k , but this is acceptable from a practical point of view. According to (23), the difference between u'_k and u_k is determined by the bias e_k^1 of the first sensor S^1 . Therefore, applying any known technique to reduce the systematic error of S^1 (e.g. sensor calibration) will make the fusion result closer to the actual humidity value.

An additional advantage of the proposed approach is its ability to estimate the discrepancy d_k . By combining (13) with various safety mechanisms that use d_k to detect sensor faults, it is possible to build fail-safe sensor fusion algorithms with high reliability.

4. Practical Aspects of Humidity Sensor Fusion with Kalman Filter

Let $d_{1:k-1} = \{d_1, d_2, \dots, d_{k-1}\}$ denote the sequence of discrepancy values $d_i, i = 1, 2, \dots, k-1$. In the Kalman filter framework, the conditional mathematical expectation:

$$E[d_k | d_{1:k-1}] = E[d_{k-1} | d_{1:k-1}] + E[\lambda_k | d_{1:k-1}] \quad (26)$$

is taken to be the best estimate $\hat{d}_{k|k-1}$ of the discrepancy at time k given all data up to $(k-1)$. Since the discrepancy d_{k-1} is fully known at time $(k-1)$, $E[d_{k-1} | d_{1:k-1}] = d_{k-1}$, and the mean of the white noise is zero, $E[\lambda_k | d_{1:k-1}] = 0$ from (26) immediately follows:

$$\hat{d}_{k|k-1} = d_{k-1} \quad (27)$$

If d_k remains constant, the predicted value will coincide with the true value. If d_k changes over time, there will be a difference between the predicted value and the true value, known as the prediction error:

$$\Delta d_k = d_k - \hat{d}_{k|k-1} = d_k - d_{k-1} \quad (28)$$

For large error values (highly variable discrepancy), the prediction model (27) is ineffective and the Kalman filter fails to accurately estimate the state variables. Using experimental data obtained from SHT31-DIS sensors, it is found that the filter works well when the prediction error Δd_k does not exceed $\pm 0,01$ RH%. How this constraint affects the design of a multi-sensor fusion system with similar sensors can be clarified using a model of SHT31-DIS [30]:

$$y_k = f y_{k-1} + (1 - f) u_{k-1} + v_{k-1} \quad (29)$$

where $f = e^{-T/\tau}$, $T = 6,29$ s is the time constant of the model, $\tau = 0,1$ s is the sampling time. For two sensors with different parameters and biases, (29) gives:

$$\begin{aligned} y_k^1 &= f^1 y_{k-1}^1 + (1 - f^1) [(1 + \alpha^1) u_{k-1} + b^1] + v_{k-1}^1 \\ y_k^2 &= f^2 y_{k-1}^2 + (1 - f^2) [(1 + \alpha^2) u_{k-1} + b^2] + v_{k-1}^2 \end{aligned} \quad (30)$$

where $f^1 = e^{-T^1/\tau}$, $f^2 = e^{-T^2/\tau}$, and T^1, T^2 denote the corresponding time constants of the models. b^1, b^2 are the additive components of the sensor errors, α^1 and α^2 are the values of the multiplicative components of the sensor errors at the end of the measurement range (when input humidity is 100 %RH), $\alpha = 0,01$ %RH⁻¹. Equations (30) define a model of the discrepancy

$$d_k = f^2 y_{k-1}^2 + (1 - f^2) [(1 + \alpha^2) u_{k-1} + b^2] - f^1 y_{k-1}^1 + (1 - f^1) [(1 + \alpha^1) u_{k-1} + b^1] \quad (31)$$

which has been used to calculate the prediction error Δd_k for step changes in humidity between 10 RH% and 60 %RH. Table 1 shows some of the results obtained for cases where the difference δT^1 and δT^2

Table 1. Prediction error of the sensor discrepancy

No	δT^1	δT^2	α^1	α^2	b^1	b^2	Δd_k
-	%	%	%RH	%RH	%RH	%RH	%RH
1	-5.00	5.00	2.50	-2.50	-2.50	2.50	-0.12
2	-5.00	5.00	2.50	0.00	-2.50	1.25	-0.10
3	-5.00	5.00	1.25	-1.25	-2.50	2.50	-0.10
4	-5.00	5.00	0.00	-2.50	-1.25	2.50	-0.10
5	-5.00	5.00	0.00	1.25	1.25	-2.50	-0.07
6	-5.00	0.00	1.25	-1.25	-1.25	2.50	-0.06
7	2.50	1.25	2.50	0.00	-2.50	1.25	-0.01
8	2.50	1.25	0.00	-1.25	0.00	2.50	0.00
9	1.25	2.50	-1.25	0.00	2.50	-1.25	0.00
10	1.25	2.50	0.00	2.50	1.25	-2.50	0.01
11	0.00	-5.00	-1.25	1.25	2.50	-2.50	0.06
12	5.00	-5.00	1.25	0.00	-2.50	1.25	0.07
13	5.00	-5.00	-2.50	0.00	2.50	0.00	0.10
14	5.00	-5.00	-1.25	1.25	2.50	-2.50	0.10
15	5.00	-5.00	0.00	2.50	1.25	-2.50	0.10
16	5.00	-5.00	-2.50	2.50	2.50	-2.50	0.12

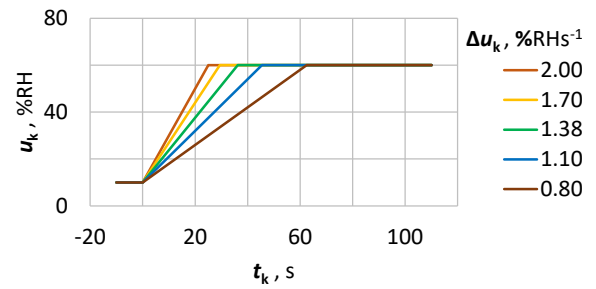


Figure 2. Signals applied to the sensor inputs. Here the humidity grows linearly from 10 %RH to 60 %RH with a rate Δu_k .

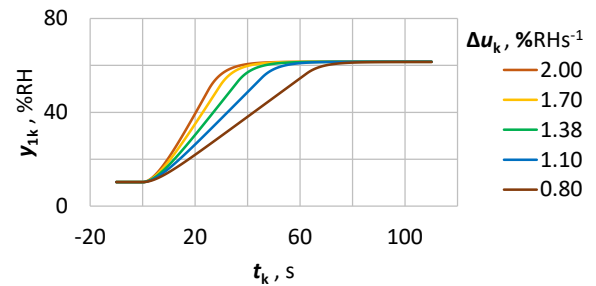


Figure 3. Output signal of sensor S^1 for case 1.

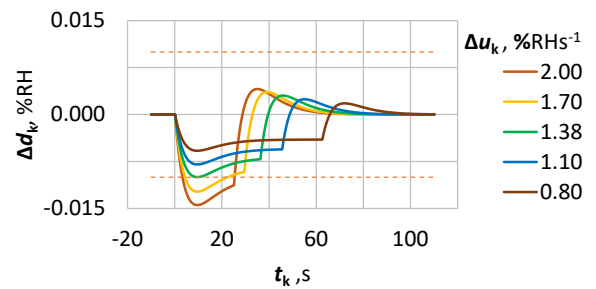


Figure 4. The prediction error calculated for case 1 of Table 1 at different input signal rates Δu_k .

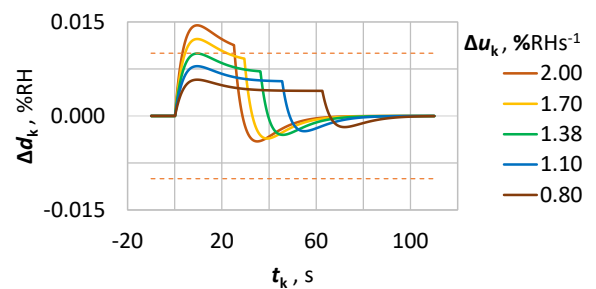


Figure 5. The prediction error calculated for case 16 of Table 1 at different input signal rates Δu_k .

between the time constants T^1, T^2 and T does not exceed ± 5 % and the additive and multiplicative error components $\pm 2,5$ %RH, respectively. For most of these cases (1-6, 11-16), the prediction error is significantly larger than that for which Kalman filter work is possible ($\pm 0,01$ RH%).

Again using (31) for the worst cases (1 and 16), Δd_k was calculated, but this time with a different rate of change of the input signal Δu_k . Figure 2 and Figure 3 depict the input and output sensor signals, and Figure 4 and Figure 5 depict the corresponding prediction errors. They show that when the rate of change of the input signal does not exceed $1,38 \text{ \%RH s}^{-1}$, the magnitude of the prediction error is less than $0,01 \text{ RH\%}$ and sensor data fusion is possible.

To validate the proposed sensor fusion, an experiment was carried out using sensors with the following parameters: $T^1 = 6,07 \text{ s}$, $a^1 = 2,07 \text{ \%RH}$, $b^1 = 0,38 \text{ \%RH}$, $T^2 = 6,31 \text{ s}$, $a^2 = -2,04 \text{ \%RH}$, $b^2 = 1,23 \text{ \%RH}$. The output signals from the sensors are shown in Figure 6 and their rate of change is shown in Figures 7 and 8.

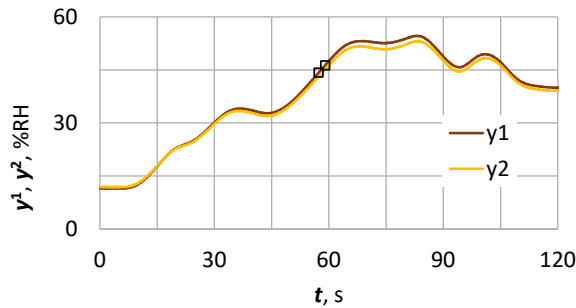


Figure 6. Response of sensors S^1 and S^2 to random changes in humidity.

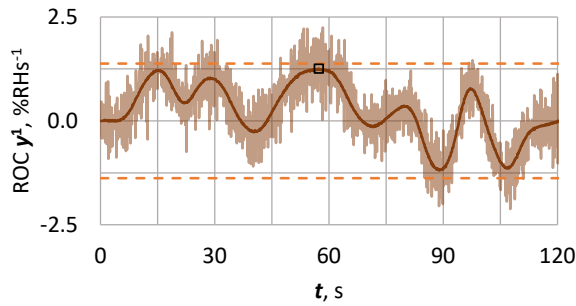


Figure 7. Rate of change (ROC) of the output y^1 of sensor S^1 . The dark brown line represents the mean value.

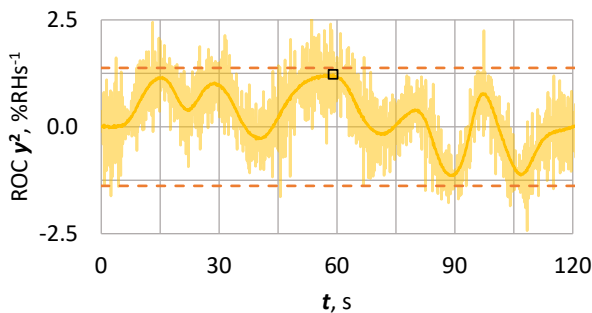


Figure 8. Rate of change (ROC) of the output y^2 of sensor S^2 . The dark yellow line represents the mean value.

The Kalman filter was started with the following polynomial model parameters $(n-1) = 2$, $q = 0,22 \text{ [\%RH]}^2 \text{ s}^{-5}$, $r_1 = 6,10^{-5} \text{ [\%RH]}^2 \text{ s}$ and $r_2 = 1,10^{-3} \text{ [\%RH]}^2 \text{ s}$. The consistency of the Kalman filter was tested using two statistical tests [29]. First, the Normalized Innovation Squared (NIS) statistic was calculated:

$$\gamma = \frac{(\mathbf{y}_k - \mathbf{H}\hat{\mathbf{x}}_{k|k-1})^T (\mathbf{H}\mathbf{P}_{k|k-1}\mathbf{H}^T + \mathbf{R})^{-1} (\mathbf{y}_k - \mathbf{H}\hat{\mathbf{x}}_{k|k-1})}{1} \quad (32)$$

and determined its lower critical value $\gamma_L = 0,05$ and upper critical value $\gamma_H = 7,38$ at significance level

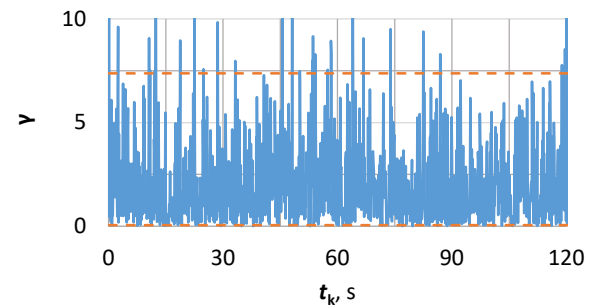


Figure 9. The normalized innovation squared (NIS) statistics.

$\alpha = 0,05$. As can be seen from Fig. 9, the test is successful as only 56 out of 1200 points (4,3 %) are outside the acceptance region. The normalized autocorrelation statistic for the components δ_1 and δ_2 of the innovation vector $\mathbf{y}_k - \mathbf{H}\hat{\mathbf{x}}_{k|k-1}$

$$\rho_1(k, l) = \frac{\sum_{i=0}^3 \delta_1(k+i)\delta_1(l+i)}{\sqrt{\sum_{i=0}^3 [\delta_1(k+i)]^2 \sum_{i=0}^3 [\delta_1(l+i)]^2}} \quad (32)$$

$$\rho_2(k, l) = \frac{\sum_{i=0}^3 \delta_2(k+i)\delta_2(l+i)}{\sqrt{\sum_{i=0}^3 [\delta_2(k+i)]^2 \sum_{i=0}^3 [\delta_2(l+i)]^2}}$$

and its thresholds $\rho_L = -0,98$ and $\rho_H = 0,98$ at the significance level $\alpha = 0,05$ were then computed. In Figures 10 and 11 they are calculated for locations

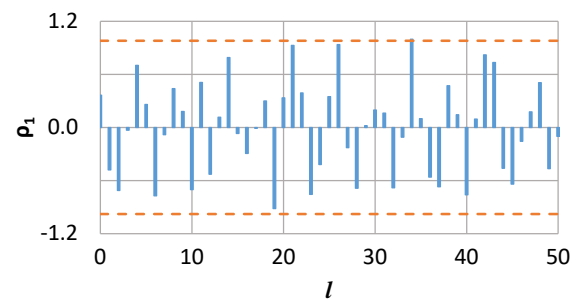


Figure 10. Normalized autocorrelation statistics for the δ_1 component of the innovation vector.

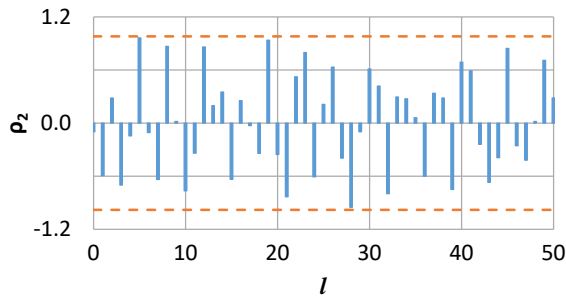


Figure 11. Normalized autocorrelation statistics for the δ_2 component of the innovation vector.

where the humidity change reaches the maximum values. All four tests are successful as the number of outliers does not exceed 1 out of 50 (2 %).

The standard deviation of the estimate of u'_k obtained by the filter in this case does not exceed 0,012 %RH and is in most cases between 1,9 and 3,3 times smaller than the standard deviation associated with the sensor measurements y_k^1, y_k^2 . Recall that the Kalman filter is an optimal linear estimator [29]. In the context of its current use, this means that it is not possible to find another sensor fusion method where the linear combination of sensor measurements yields a result with a smaller error.

The performance of the filter is shown in Figures 12-15. The sensor discrepancy calculated by the filter is shown in Figure 12.

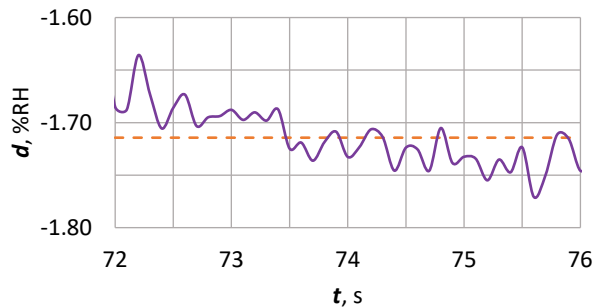


Figure 12. Plot of estimated humidity sensor discrepancy d_k over time.

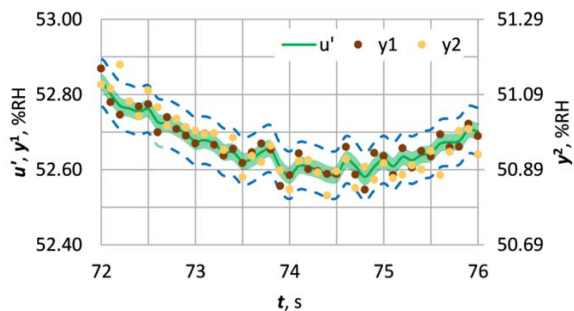


Figure 13. Humidity u'_k calculated by the filter and the measurements obtained from the sensors.

In the time interval 72 s – 76 s its average value is approximately 1,71 %RH. This value has been used to shift the origin of the coordinate system in which the measurements obtained by the second sensor S^2 are shown (Figure 13). This makes it easy to see the scatter in the measurements (the area bounded by the dashed curves) caused by random sensor errors. The mean value of u'_k and its uncertainty are shown in green. It has already been noted that the difference between the humidity u'_k calculated by the filter and the actual humidity u_k is determined solely by the systematic error of the first sensor S^1 . This can be clearly seen in Figure 14. Calibration of sensor S^1 solves this problem (Figure 15).

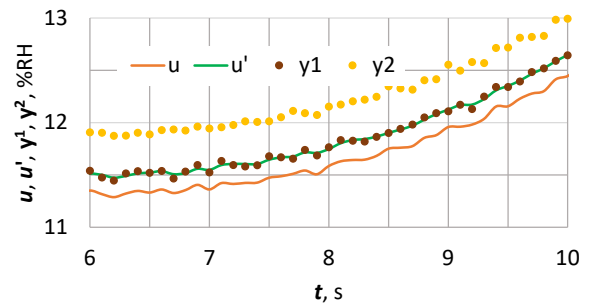


Figure 14. Real humidity u_k and humidity u'_k calculated by the filter before calibration of sensor S^1 .

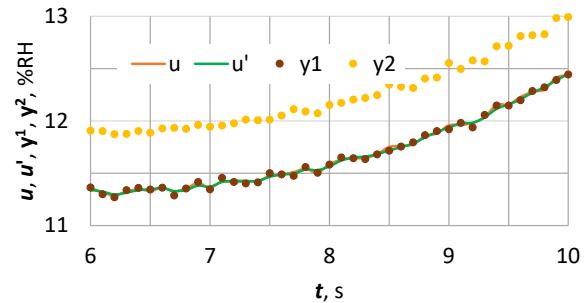


Figure 15. Real humidity u_k and humidity u'_k calculated by the filter after calibration of sensor S^1 .

5. Conclusion

Fusion of sensor signals is not a trivial task. Typically, signals are generated by non-stationary random processes, which implying that there is some relationship between their current and past values. Most classical fusion algorithms are static, since they combine observations from different sources obtained only at the present moment, but cannot use information from previous observations to improve the fusion result. The Bayesian approach is one of the few that provides a clear theoretical framework to address this problem.

This, together with the possibility of real-time implementation by a simple numerical procedure (Kalman filter), makes it a leading method for sensor fusion.

The application of the Bayesian fusion approach implies the use of a discrete model in the state space. In the classical case, this means collecting information about the phenomenon in advance, then selecting a model and determining its parameters. Polynomial models are a special type of model that allows this process to be greatly simplified. Here, most of the model parameters are embodied in the state vector and estimated in real time from the incoming data, while the remaining parameters (model order, process and measurement noise intensities) are adjusted in the Kalman filter tuning process. The results of the present study fully confirm the applicability of this procedure when a polynomial model with a local quadratic trend is used to represent humidity sensor signals.

In general, Bayesian fusion with a Kalman filter assumes that all sensors are calibrated and the resulting observations are free of systematic errors. By augmenting the polynomial model of the signal with a random walk model of the sensor discrepancy, a solution is found where fusion is possible if only one of the sensors in the measurement system is calibrated. However, the use of a random walk model in this case imposes certain requirements on the sensors and the input signal, the performance of which guarantees the consistency of the estimates obtained by the Kalman filter. Theoretical analysis and experimental data show that when using SHT31-DIS sensors with a time constant tolerance and a multiplicative error not exceeding $\pm 5,0\%$ and $\pm 2,5\%$ RH respectively, normal operation of the Kalman filter is possible if the rate of change of the input signal (humidity) does not exceed $1,38\%RHs^{-1}$. This limitation is acceptable in many cases as it represents a situation where the humidity would increase from 0 RH% to 100 RH% in just over a minute.

The results obtained provide a reason to define the combination of polynomial model and Bayesian fusion algorithm as a useful tool for the design of accurate, reliable and easy to implement and operate multi-sensor measurement systems. Presented as a solution to the problem of fusing two humidity sensors, this approach can be applied to any other measurand or number of sensors.

References:

- [1]. Hyndman, R. J., & Athanasopoulos, G. (2018). *Forecasting: principles and practice*. OTexts.
- [2]. Aguado-Rodríguez, G. J., Quevedo-Nolasco, A., Castro-Popoca, M., Arteaga-Ramírez, R., Vázquez-Peña, M. A., & Zamora-Morales, B. P. (2016). Meteorological variables prediction through ARIMA models. *Agrociencia*, 50(1), 1-13.
- [3]. Murat, M., Malinowska, I., Gos, M., & Krzyszczak, J. (2018). Forecasting daily meteorological time series using ARIMA and regression models. *International agrophysics*, 32(2).
- [4]. Naseem, F., Rashid, A., Izhar, T., Khawar, M. I., Bano, S., Ashraf, A., & Adnan, M. N. (2018). An integrated approach to air pollution modeling from climate change perspective using ARIMA forecasting. *Journal of Applied Agriculture and Biotechnology*, 2(2), 37-44.
- [5]. Liu, T., & You, S. (2022). Analysis and Forecast of Beijing's Air Quality Index Based on ARIMA Model and Neural Network Model. *Atmosphere*, 13(4), 512.
- [6]. Mancini, S., Francavilla, A., Graziuso, G., & Guarnaccia, C. (2022). An Application of ARIMA modelling to air pollution concentrations during covid pandemic in Italy. In *Journal of Physics: Conference Series*, 2162(1), 012009. IOP Publishing.
- [7]. Kumar, U., & Jain, V. K. (2010). ARIMA forecasting of ambient air pollutants (O₃, NO, NO₂ and CO). *Stochastic Environmental Research and Risk Assessment*, 24, 751-760.
- [8]. Manco-Perdomo, L. A., Pérez-Padilla, L. A., & Zafra-Mejía, C. A. (2021). Intervention analysis with autoregressive integrated moving average models for time series of urban air pollutants. In *Journal of Physics: Conference Series*, 2139(1), 012002. IOP Publishing.
- [9]. Muzalyova, A., Brunner, J. O., Traidl-Hoffmann, C., & Damialis, A. (2021). Forecasting Betula and Poaceae airborne pollen concentrations on a 3-hourly resolution in Augsburg, Germany: toward automatically generated, real-time predictions. *Aerobiologia*, 37, 425-446.
- [10]. Arca, B., Pellizzaro, G., Canu, A., & Vargius, G. (2002). Airborne pollen forecasting: Evaluation of ARIMA and neural network models. In *15th Conference on Biometeorology and Aerobiology, Kansas City, MO, USA, P, 3*.
- [11]. Durbin, J., & Koopman, S. J. (2012). *Time series analysis by state space methods*, 38. OUP Oxford.
- [12]. Plamen Nikovski, Tanya Titova, Nikolay Doychinov.(2022). Application of the Weierstrass Theorem for Sensors Signal Modelling. *TEM Journal*, 11(4), 1423-1431.
- [13]. Harvey, A. (2010). The local quadratic trend model. *Journal of Forecasting*, 29, 94-108.

- [14]. Broer, A. A., Benedictus, R., & Zarouchas, D. (2022). The Need for Multi-Sensor Data Fusion in Structural Health Monitoring of Composite Aircraft Structures. *Aerospace*, 9(4), 183.
- [15]. Molino-Minero-Re, E., Aguilera, A. A., Brena, R. F., & Garcia-Ceja, E. (2021). Improved Accuracy in Predicting the Best Sensor Fusion Architecture for Multiple Domains. *Sensors*, 21(21), 7007.
- [16]. Gai, Y. L., & Wang, Y. P. (2013). Data fusion and Bayes estimation algorithm research. *Applied Mechanics and Materials*, 347, 2620-2624.
- [17]. Ahmed, M., & Pottie, G. (2004). Fusion in the context of information theory. *Distributed sensor networks*, 419.
- [18]. Li, H. (2014). A Brief Tutorial On Recursive Estimation With Examples From Intelligent Vehicle Applications (Part I): Basic Spirit And Utilities. *HAL open science*.
- [19]. Fang, H., Tian, N., Wang, Y., Zhou, M., & Haile, M. A. (2018). Nonlinear Bayesian estimation: From Kalman filtering to a broader horizon. *IEEE/CAA Journal of Automatica Sinica*, 5(2), 401-417.
- [20]. Sneyd, J., Fewster, R. M., & McGillivray, D. (2022). The total probability rule. In *Mathematics and Statistics for Science*, 605-620. Springer, Cham.
- [21]. Mitchell, H. B. (2012). *Data fusion: concepts and ideas*. Springer Science & Business Media.
- [22]. Mensing, C., Sand, S., & Dammann, A. (2010). Hybrid Data Fusion and Tracking for Positioning with GNSS and 3GPP-LTE. *International Journal of Navigation & Observation*.
- [23]. Zhang, P., Zhou, S., Liu, P., & Li, M. (2022). Distributed Ellipsoidal Intersection Fusion Estimation for Multi-Sensor Complex Systems. *Sensors*, 22(11), 4306.
- [24]. Åström, K. J., & Wittenmark, B. (2013). *Computer-controlled systems: theory and design*. Courier Corporation.
- [25]. Dybko, A. (2001). Errors in chemical sensor measurements. *Sensors*, 1(1), 29-37.
- [26]. Dichev, D., Zhelezarov, I., & Madzharov, N. (2021). Dynamic Error and Methods for its Elimination in Systems for Measuring Parameters of Moving Objects. *Transactions of FAMENA*, 45(4).
- [27]. Gamse, S. (2018). Dynamic modelling of displacements on an embankment dam using the Kalman filter. *Journal of Spatial Science*, 63(1), 3-21.
- [28]. Farrell, J. (2008). *Aided navigation: GPS with high rate sensors*. McGraw-Hill, Inc.
- [29]. Bar-Shalom Y, Li X & Kirubarajan T. (2004). *Estimation with Applications to Tracking and Navigation: Theory Algorithms and Software*. New York: John Wiley & Sons.
- [30]. Nikovski, P., & Doychinov, N. (2021). A Prediction Model of Humidity Sensor Response. In *2021 XXX International Scientific Conference Electronics (ET)*, 1-4. IEEE.